Chemistry Europe
European Chemical Societies Publishing

Conjugated Polymers with Aggregation-Induced Emission Characteristics for Fluorescence Imaging and Photodynamic Therapy

Lirong Wang,[a] Rong Hu,[a] Anjun Qin,*[a] and Ben Zhong Tang[a, b]

Accurate diagnosis and treatment have been extensively developed in the field of biomedicine, which put forward higher requirements for the development of biomedical materials with high efficiency and selectivity. Among them, conjugated polymers featuring aggregation-induced emission (AIE) characteristics (AIE conjugated polymers) have stood out in recent years owing to their unique properties, such as intense solid emission, high light-harvesting ability, efficient energy transfer, and high $^1O_2$ generation ability, which empower them with effective biomedical functions in fluorescence imaging (FLI), photodynamic therapy (PDT), FLI-guided PDT, two-photon excited photodynamic therapy (2PE-PDT), *etc.* In this review, we highlight recent progress in AIE conjugated polymers and their applications in anticancer and antibacterial areas based on FLI and PDT, and summarize the mechanism of color-tuned fluorescence emission and efficient $^1O_2$ generation ability. The challenges and perspectives for the future development of AIE conjugated polymers are also discussed.

1. Introduction

The rapid growth and high mortality of cancer along with serious diseases caused by pathogenic bacteria have been threating the human health.[1] It is particularly urgent to develop accurate diagnostic techniques and efficient treatment methods to overcome them. Compared with conventional theranostic strategies, photodynamic therapy (PDT) has received growing attention owing to its high spatiotemporal accuracy and low drug-resistance. Reactive oxygen species (ROS), as the critical proportion of PDT, mainly includes free radicals ($O_2^{\bullet-}$ and $^{\bullet}OH$, *etc.*, type I) and singlet oxygen ($^1O_2$, type II), which can destroy the structure and functions of biomolecules, resulting in the efficient killing of cancer cells.[2] Compared with type II ROS, type I ROS can overcome hypoxic and realize more extensive anti-tumor applications. In general, effective photosensitizers (PSs), opportune light and sufficient oxygen molecules (O_2) are essential factors for efficient $^1O_2$ generation. Due to the good biocompatibility, organic PSs are highly demanded and have been approved by Food and Drug Administration (FDA), USA for clinical application. So for, three generations of PSs mainly including porphyrin and chlorin structure or their derivatives have been systematically investigated for preclinical studies.[3] However, critical issues, such as poor water-solubility and photo-bleaching, have severely hindered their further applications in clinic therapy.[4] By taking advantage of the strong light-harvesting ability and efficient energy transfer effect, PSs based on conjugated polymers (CPs) hold great potential for imaging and PDT applications.[5] In general, the low mass molecular PSs could realize the generation of typical type I or type II ROS through special design.[2e,f] Whereas, for CPs, there is few work to report the pure type I or type II PSs. Moreover, conventional CPs generally suffer from the reduced ROS generation and aggregation-caused quenching (ACQ) when forming aggregates in aqueous solution, which impede their prospective applications in biomedical fields.[6]

Fortunately, PSs featuring aggregation-induced emission (AIE) characteristics offer a straightforward strategy to solve these problems. Opposite to the ACQ effect, AIE luminogens (AIEgens) usually exhibit intense fluorescence in concentrated solution or aggregate state due to the inhibition of nonradiative decay through the restriction of intramolecular motion (RIM).[7] Currently, numerous AIEgens have be designed for diverse applications, such as in the fields of optoelectronic devices, bioimaging, and therapy.[8] Notably, PSs featuring AIE activity always show enhanced ROS generation effect upon the formation of aggregates because the RIM blocks the nonradiative decay pathways, which has been verified by several works.[2b,9] By introducing AIEgens into the skeleton of CPs, AIE conjugated polymers can be efficiently constructed.[10] Therefore, such polymers not only possess the merits of AIE with intense emission and high ROS generation ability in aggregate state, but also own the superiorities of CPs with strong light-harvesting ability and effective energy transfer (Figure 1a). Among these advantages, the AIE feature and effective energy transfer endow AIE conjugated polymers with great potential in fluorescent imaging (FLI) with color-tuned emission and out-

[a] *Dr. L. Wang, Dr. R. Hu, Prof. A. Qin, Prof. B. Z. Tang*
State Key Laboratory of Luminescent Materials and Devices
Guangdong Provincial Key Laboratory of Luminescence from Molecular Aggregates
Center for Aggregation-Induced Emission
South China University of Technology
Guangzhou 510640 (China)
E-mail: msqinaj@scut.edu.cn
[b] *Prof. B. Z. Tang*
Shenzhen Institute of Aggregate Science and Technology
School of Science and Engineering
The Chinese University of Hong Kong
Shenzhen, 518172 (China)

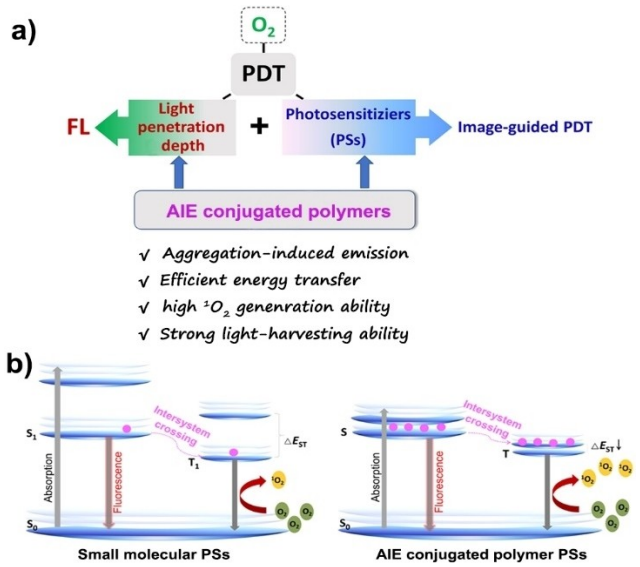

Figure 1. (a) The main factors of photodynamic therapy (PDT) and the advantages of AIE conjugated polymers. (b) Working mechanism of low mass molecular photosensitizers (PSs) and AIE conjugated polymer based PSs.

standing photostability. Furthermore, AIE conjugated polymers with stronger light-harvesting abilities have small difference of the lowest excited singlet and triplet states ($\Delta E_{S\text{-}T}$), facilitating intersystem crossing (ISC) process to generate more $^1O_2$ compared with low mass molecular PSs (Figure 1b), which empower them with synergistic effect for FLI-guided PDT applications.

In 2014, Wang et al.[10a] presented an excellent review on the design and synthesis of AIE conjugated polymers. Until now, many new AIE conjugated polymers have been reported for diverse applications. In this review, we will mainly outline the recent progress in new applications of AIE conjugated polymers in FLI and PDT with comparing and discussing their superiorities over low mass PSs in details. In the conclusion part, we summarize the reasons of high-performance emission and $^1O_2$ generation ability of AIE conjugated polymers. Finally, perspectives about the future development of AIE conjugated polymers and their biomedical applications are presented.

2. Applications of AIE Conjugated Polymers

Thanks to the AIE feature and π conjugated structures, AIE conjugated polymers possess synergistic effects in fluorescence emission, quantum yields and ROS generation capability, which endow them with color-tuned FR/NIR emission and higher ROS generation efficiency compared with low-mass PSs, realizing *in vitro* and *in vivo* FLI, and FLI guided PDT in anticancer and antibacterial applications.

Lirong Wang received her Ph.D. degree from the Department of Chemistry and Engineering, Xiamen University in 2018. She is now conducting her postdoctoral research with co-supervisors Anjun Qin and Ben Zhong Tang at South China University of Technology. Her current research focuses on the development of dual-modal imaging guided phototherapy based on magnetic resonance imaging (MRI) and aggregation-induced emission (AIE).

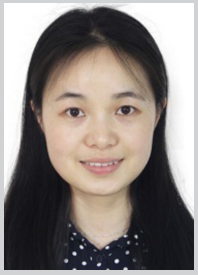

Rong Hu received her Ph.D. degree from the Institute of Chemistry, Chinese Academy of Sciences in 2016. She conducted her postdoctoral research with co-supervisors Anjun Qin and Ben Zhong Tang at South China University of Technology in 2016–2019. After that, she was a visiting scholar at the Hong Kong University of Science and Technology in 2019–2020. Her current research focuses on the development of AIE-active polymer and its application in biomedicine.

Professor Anjun Qin received his Ph.D. degree from the Institute of Chemistry, Chinese Academy of Sciences in 2004. He conducted his postdoctoral research under the supervision of Ben Zhong Tang in the Department of Chemistry, Hong Kong University of Science and Technology and the Department of Polymer Science and Engineering, Zhejiang University in 2005-2008. Then, he was promoted to associate professor at Zhejiang University. From 2013, he has been at the South China University of Technology and was promoted to professor. His research interests include synthetic polymer chemistry and organic/polymer functional materials.

Professor Ben Zhong Tang received his Ph.D. degree from Kyoto University in 1988. He conducted his postdoctoral work at University of Toronto in 1989-1994. After that, he joined Hong Kong University of Science and Technology in 1994 and was promoted to Chair Professor in 2008 and Stephen K. C. Cheong Professor of Science in 2013. In 2021, he joined The Chinese University of Hong Kong, Shenzhen. In 2001, he coined the concept of aggregation-induced emission (AIE). His research interests include the exploration of new advanced materials, new luminescent processes and new polymerization reactions.

2.1. Fluorescence imaging (FLI)

Owing to the high sensitivity and simple operation, FLI has attracted great interest of scientists in sensing area. For most of conventional fluorophores, they usually suffer from serious photo-bleaching and ACQ effect, which restrict their further biological applications. Opposite to this, AIE conjugated polymers with high light-harvesting capability, excellent photostability and high fluorescence quantum yields (QYs) possess obvious advantages for cell imaging and color-tuned FR/NIR tumor imaging.

Our group has successfully designed and prepared an AIE conjugated polymer of P(TPE-2OEG) by Suzuki polycoupling, which contains mainly three parts, that is, conjugated backbone, tetraphenylethene (TPE) units and oligo(ethylene glycol)s (OEGs) side-chain (Figure 2a).[11] Interestingly, P(TPE-2OEG) could selectively turn on the live cells. As a sharp contrast, its monomer of M(TPE-2OEG) and low mass Calcein AM can label viable cells, apoptotic and dead cells at the same time (Figure 2b), Demonstrative of the advantage of our polymer over low mass molecules in viable cell discrimination. This should be attributed to the unique structure of P(TPE-2OEG), of which conjugated backbone and TPE units endowed P(TPE-2OEG) with high light-harvesting ability and unique photophysical properties. More importantly, the side chains of OEGs with negative charge ensured P(TPE-2OEG) to have good biocompatibility and reduce the nonspecific interaction with cell membrane, which made it specifically label living cells by endocytosis. Meanwhile, due to the lack of enough energy for uptake of P(TPE-2OEG), apoptotic cells or dead cells would not be labeled.

By changing the side chains from OEGs to ethylenediaminetetraacetic acid (EDTA) and the co-monomer of TPE from phenyl to benzothiadiazole units, Zhang, Qin and coworkers prepared a new AIE conjugated polymer of PTB-EDTA by Suzuki polycoupling, which could be used to *in situ* monitor the process of osteogenic differentiation (Figure 2c).[12] The EDTA moieties of PTB-EDTA offer it excellent solubility, biocompatibility, and high affinity towards Ca^{2+}, which are vital metal element for osteogenic differentiation. Different from its low-mass model compound of MTB-EDTA, the polymer could effectively chelate Ca^{2+} and cross the cell membrane by endocytosis, resulting in selective enrichment in osteoblasts. Moreover, PTB-EDTA is more sensitive than Alizarin Red S staining for detection of osteogenic differentiation, in which the fluorescence of polymer was detectable at the 7th day of differentiation (Figure 2d). However, the signal could only be recorded at the 14th day for Alizarin Red S staining. Therefore,

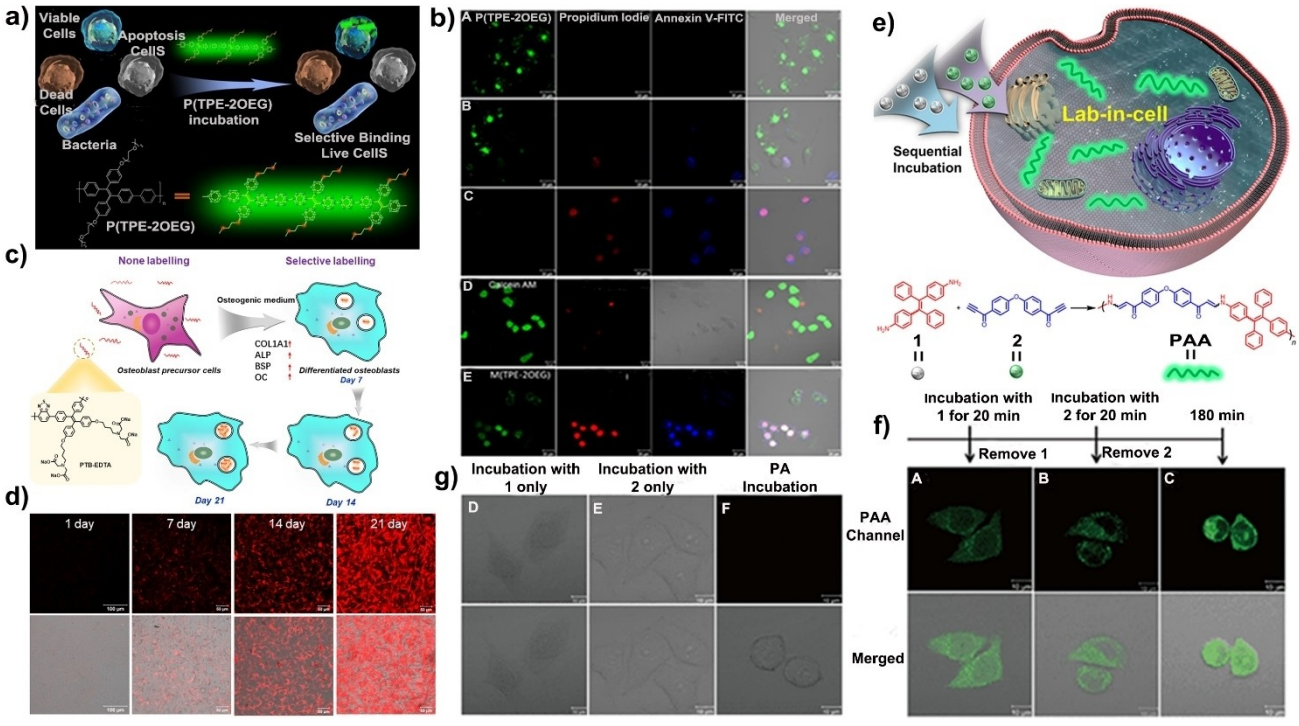

Figure 2. *In vitro* Fluorescent imaging. (a) Schematic illustration of selectively discrimination of viable cells from apoptosis cells, dead cells and bacteria and the molecular structure of P(TPE-2OEG). (b) CLSM of HeLa cells incubated with P(TPE-2OEG) (A–C), Calcein AM (D), and M(TPE-2OEG) (E), respectively. A–C: HeLa cells treat with 0, 500, 1000 μM H_2O_2. D and E: HeLa cells treat with 500 μM H_2O_2. Reproduced with permission from Ref. [11]. Copyright (Elsevier), 2020. (c) The chemical structures of PTB-EDTA and cartoon illustration of its cellular internalization and high sensitivity for real-time detection of osteogenic differentiation. (d) Cell imaging of MC3T3-E1 incubated with PTB-EDTA for 12 h at indicated differentiation time. Reproduced with permission from Ref. [12]. Copyright (John Wiley & Sons Inc.), 2020. (e) Illustration of the intracellular spontaneous amino-yne click polymerization, and synthetic route to poly(β-aminoacrylate) (PAA). (f) CLSM images of HeLa cells incubated with 1 for 20 min (A), followed by removal of 1 and incubation with 2 for 20 min (B), and the long-term incubation after the removal of 2 in the medium for additional 140 min (C). (g) CLSM of HeLa cells incubated with **1** (D), **2** (E), and pre-prepared PAA (F) for 140 min. Reproduced with permission from Ref. [13]. Copyright (Springer Nature), 2019.

PTB-EDTA holds great potential for evaluating osteogenic differentiation and related applications.

Besides using traditional polymerizations, we also synthesized AIE conjugated polymers by employing our established efficient click polymerizations. For example, we used our developed spontaneous amino-yne click polymerization to synthesize AIE polymers. Thanks to its high efficiency, metal-free and spontaneous feature, and mild reaction conditions, we successfully established a lab-in-cell. In other words, the click polymerization was carried in living cells, which could be used to turn on and kill the cells (Figure 2e).[12] By systematically investigating the *in vitro* click polymerization conditions, it had been proved that the TPE containing diamine (**1**) could spontaneously polymerize with the carbonyl group activated terminal diyne (**2**) in cells under physiological conditions, and an AIE polymer PAA with weight-average molecular weight (M_w) of 7300 was generated. Interestingly, after polymerization, the cells were "turned on" (Figure 2f). In contrast, if cells were only incubated with the monomer **1** or **2** or pre-prepared PAA, there was no fluorescent signal and M_w could be detected inside cells (Figure 2g), which means that no organic products with high M_w existed in these cells. Additionally, the intracellularly formed polymers could destroy the structures of actin and tubulin in the cytoplasm and lead to the cell death, highlighting that this strategy of intracellular spontaneous amino-yne click polymerization could be used to realize drug-free therapy in the future. This work extends the application of click polymerization in biological science and provides great prospect to develop a powerful tool for bioimaging and therapy.

With above mentioned polymerizations, how to design a far-red/near infrared (FR/NIR) fluorescence probe is the direction that researchers have been working hard on. FR/NIR fluorescence imaging is indispensable mode for bioimaging due to low autofluorescence background and better light penetration depth. AIE conjugated polymers with high light-harvesting ability and efficient energy transfer are conducive to the occurrence of fluorescence resonance energy transfer (FRET), which can tune fluorescence emission from blue to deep red or even NIR. Yuan *et al.*[14] reported two color-tunable AIE conjugated polymer nanoparticles by tuning their intramolecular FRET processes. As shown in Figure 3a, P-**1** with only one intramolecular FRET process exhibited a clear green-colored fluorescence. After the second intramolecular FRET pair was added to P-**2**, the fluorescence color was tuned from green to

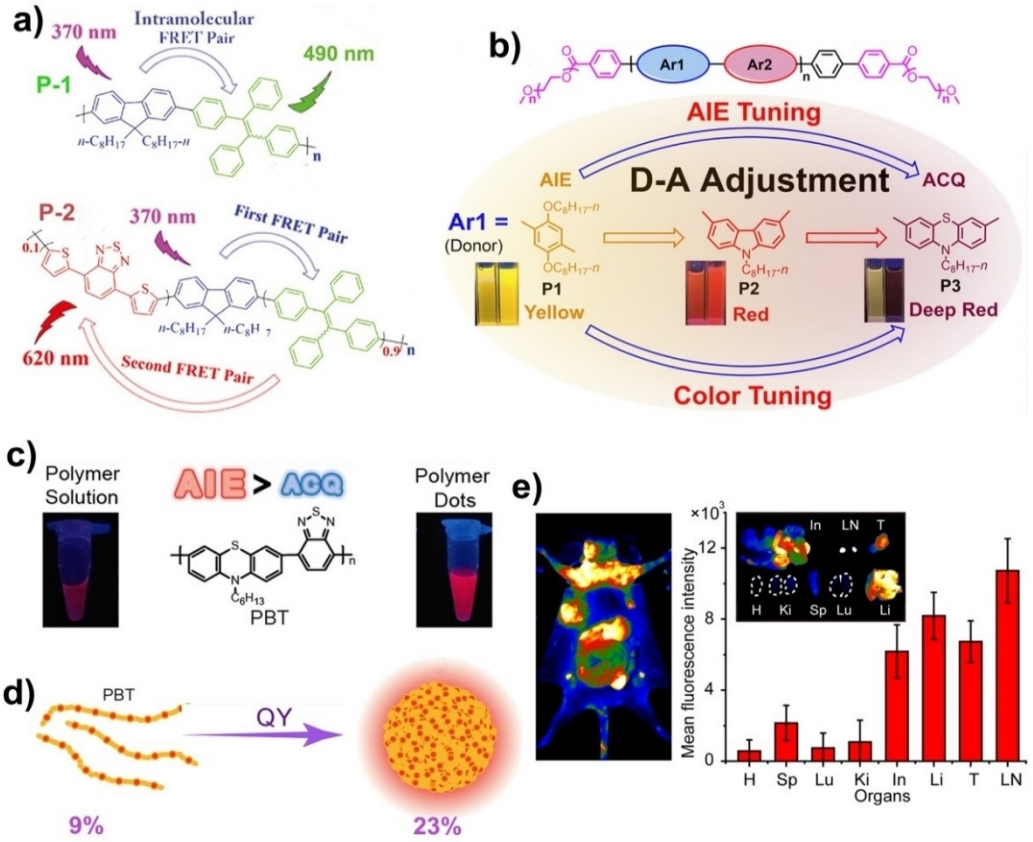

Figure 3. Color-tuned Red and near infrared (NIR) fluorescence imaging. (a) Two color tunable AIE conjugated polymers by tuning their intramolecular FRET pairs. P-1 contains one FRET pair with green emission at 490 nm, and the second intramolecular FRET pair was added in P-2 with red fluorescence emission (620 nm). Reproduced with permission from Ref. [14]. Copyright (Royal Society of Chemistry), 2018. (b) Schematic diagram of three AIE conjugated polymers P**1**-P**3** with AIE and colored tuning ability by adjusting the donor structure. Reproduced with permission from Ref. [15]. Copyright (American Chemical Society), 2019. (c) The molecular structure of AIE conjugated polymers PBT and the comparison of fluorescence of polymers solution and polymer dots. (d) The enhancement of fluorescence QY of PBT polymer dots. (e) *In vivo* tumor and *ex vivo* imaging, and mean fluorescence intensity of tissues and tumor. Reproduced with permission from Ref. [16]. Copyright (American Chemical Society), 2020.

red. Later, Yuan, Hua and coworkers reported three color tunable and amphipathic AIE conjugated polymers with TPE moiety and donor-acceptor (D–A) type electronic structure, P**1** to P**3**.[15] The fluorescence of P**1** to P**3** could be tuned from AIE to ACQ, and the emissive color could be easily adjusted from yellow to deep red by choosing stronger electronic donors successively (Figure 3b). Due to the AIE and amphiphilic property, P**1** and P**2** could be engineered into polymer dots (Pdots) to delivery anticancer drug paclitaxel and image their location by yellow- or red-colored fluorescence signal. Especially, the Pdots of P**2** exhibited the similar level in *in vivo* antitumor efficacy compared with clinical anticancer drug Abraxane® without emissive property. This work demonstrated the significance of application of AIE conjugated polymers with D–A-type structure in the design of self-illuminating drug delivery systems.

Recently, Wu and coworkers[16] reported NIR emissive AIE conjugated polymers PBT with high fluorescence QY (Figure 3c). After fabricating PBT into Pdots, the fluorescence QYs were further improved from 9% to 23% (Figure 3d). By virtue of outstanding fluorescence properties and biocompatibility, PEGylated PBT dots were used for *in vivo* imaging. As shown in the Figure 3e, the tumor area exhibited an intense fluorescence signal and clearly discernible margins due to the enhanced permeability and retention (EPR) effect, apart from liver and intestine, which revealed the remarkable potential of the PBT dots for tumor imaging.

2.2. FLI-guided PDT for antitumor applications

Imaging-guided PDT has become one of the most attractive research fields because it can realize precise locating of tumors and continuous *in vivo* tracking of theranostic agents, which will instruct the oncologists to apply irradiation light at appropriate time point.[18] Undoubtedly, effective image-guided PDT is inseparable from ideal photosensitizers with both photostable FR/NIR fluorescence and sufficient ROS generation capability. Thanks to their advantages of enhanced fluorescence intensity and ROS generation ability, AIE-active PSs are suitable for FLI-guided PDT. To realize "both in one" photosensitizer, AIE conjugated polymers with strong donor (D) and acceptor (A) units would be the best choice. Liu and coworkers[6] reported such a FR/NIR conjugated polymer with AIE feature and good ROS generation ability (Figure 4a). In this AIE conjugated polymer, TPE and anthraquinone (AQ) moieties were used as

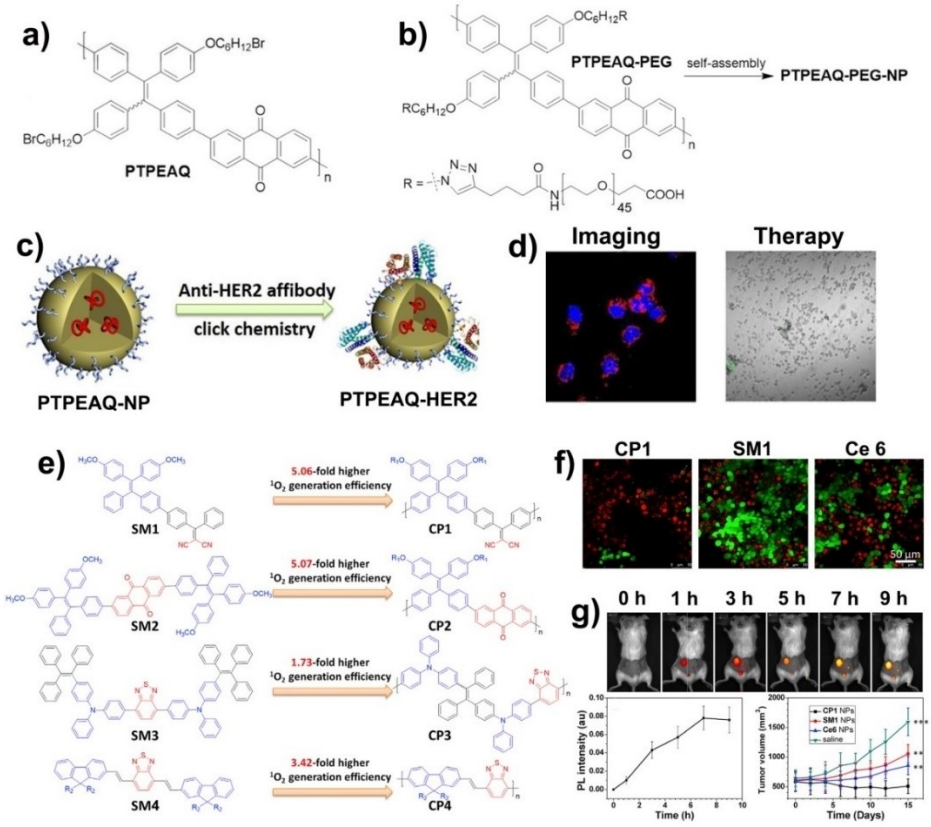

Figure 4. AIE conjugated polymers with FR/NIR emission and higher $^1O_2$ generation ability compared with small molecular PSs for imaging-guided PDT. (a and b) The molecular structures of PTPEAQ and PTPEAQPEG. (c) The modification of PTPEAQ-NP with anti-HER2 affibody by click chemistry toward PTPEAQ-NP-HER2. (d) Imaging and therapy of SKBR-3 cancer cells with PTPEAQ-NP-HER2. Reproduced with permission from Ref. [6], Copyright (American Chemical Society), 2016. (e) The chemical structures of CPs (CP1 ~ CP4) with higher $^1O_2$ generation efficiency compared with corresponding small molecules (SM1 ~ SM4). (f) The imaging of cancer cells PDT of CP1, SM1 and Ce6. (g) Imaging-guided PDT of CP1 for tumor eradication in vivo. Reproduced with permission from Ref. [17]. Copyright (John Wiley & Sons Inc.), 2018.

the strong D and A respectively to make the resultant PTPEAQ FR/NIR emission with the wavelength of 680 nm. As comparison, the authors modified PTPEAQ with PEG unit (PTPEAQPEG-NP) to certificate that PTPEAQ-NP had higher performance in both fluorescence and ROS generation due to the tighter packing status (Figure 4b). In order to realize the targeting and imaging-guided PDT cancer cell ablation, they conjugated the anti-HER2 affibody to the surface of PTPEAQ-NP to obtain PTPEAQ-NP-HER2 (Figure 4c), which could be selectively internalized into SKBR-3 cancer cells and kill them under white light irradiation (Figure 4d). This is the first report about AIE conjugated polymers with FR/NIR fluorescence imaging to guide efficient PDT of cancer cells.

Afterward, their group went on to explore why AIE conjugated polymers could improve the capability of $^1O_2$ generation. They found that AIE conjugated polymers could generate more $^1O_2$ compared with corresponding low mass molecules and termed this strategy as ''polymerization-enhanced photosensitization'' effect.[17,19] This is mainly attributed to the improved ISC process and enhanced light-harvesting ability of CPs. As shown in Figure 4e, among these AIE conjugated polymers, CP1 showed the highest $^1O_2$ generation efficiency in aqueous media, which was 5.06-fold higher than SM1 under white-light irradiation (60 mW/cm^2, 400–700 nm). Taking advantage of such high $^1O_2$ generation efficiency, they utilized CP1 NPs to achieve the photodynamic cancer cell ablation (Figure 4f) and image-guided tumor PDT (Figure 4g). Additionally, SM4 and CP4 were non-AIE systems, but CP4 had still 3.42-fold higher $^1O_2$ generation efficiency than low mass SM4 (Figure 4e), which indicated that polymerization-enhanced photosensitization was also effective in a non-AIE system and expanded the scope of this concept.

Besides the strength of D and A units, Tang and coworkers found that the number of D and A units could also facilitate the photosensitization.[20] They synthesized several AIEgens based on electron donating triphenylamine (T) and electron-accepting benzothiadiazole (B) units. As depicted in Figure 5a, with an increase in conjugation from TB to P1, the $^1O_2$ quantum yield (Φ_o) increased from 3.8% to 14%, accompanied with a decreased fluorescence quantum yield (Φ_f) from 87% to 7%. This inverse correlation between Φ_o and Φ_f suggested that the increasing conjugation by polymerization was an effective way to enhance ISC. Moreover, if the number of A unit was more than that of D unit in the molecular structure, the D–A conjugated AIEgens would obtain a stronger photosensitization (Figure 5a). With these two strategies of the polymerization method and D–A even-odd effect, the Φ_o of the AIEgens can be increased by 5.8- and 2.7-fold, respectively, which was attributed to the enhancement of ISC for more $^1O_2$ generation (Figure 5b). For *in vitro* and *in vivo* application, P**1** NPs were prepared by encapsulating P**1** to amphiphilic DSPE-PEG2000. The result of CLSM showed P**1** NPs were mainly located in the mitochondria (Figure 5c). With the excellent photosensitization ability and fluorescence property, P**1** NPs were applied to conduct the FLI-guided PDT under white light irradiation successfully (Figure 5d). Overall, using these strategies reasonably to design novel PSs could acquire excellent-efficiency PSs.

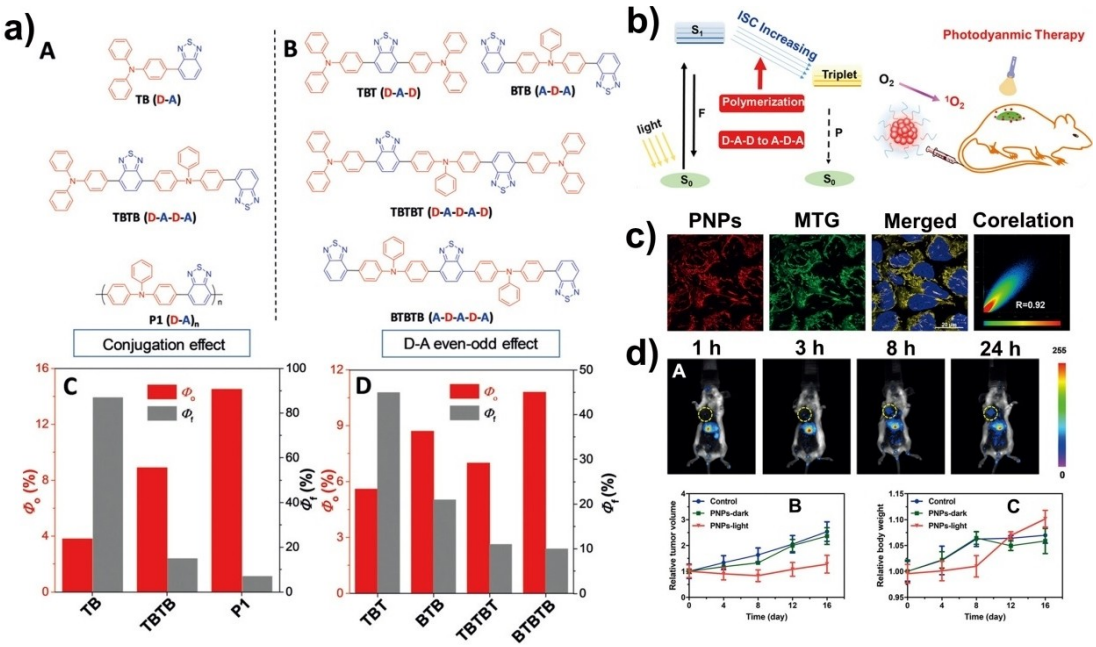

Figure 5. The photosensitizers with different D–A-D to A–D-A structure to enhance photosensitization for *in vivo* imaging-guided PDT. (a) Molecular structures (A and B), $^1O_2$ quantum yield and fluorescence quantum yield (C and D) of TB, TBTB, and P1 and TBT, BTB, TBTBT, and BTBTB, respectively. (b) Schematic illustration of the polymerization and even-odd effect to enhance photosensitization for application in PDT. (c) Colocalization images *in vitro*. (d) *In vivo* imaging-guided PDT. (A) *In vivo* FL;(B) Tumor growth curves and (C) body weight changes of mice in different treatment groups. Reproduced with permission from Ref. [20]. Copyright (John Wiley & Sons Inc.), 2018.

2.3. Two-photon excited PDT for antitumor applications

The PDT effect of most of AIE conjugated polymers were generated through white-light irradiation, which restricted the efficiency of *in vivo* PDT in some degree because of the limited tissue penetration depth of white light. Different from the white light excited PDT, two-photon excited one (2PE-PDT) has aroused many researchers' interests in recent years owing to its great potential for deep-tissue and spatiotemporally accurate cancer therapy.[21] However, the availability of PSs with large two-photon absorption (2PA) cross section and high ROS generation efficiency greatly limits the advancement of 2PE-PDT.[22] Moreover, for low mass AIE PSs with two-photon excitation, it is difficult to achieve both high 2PA cross-section and $^1O_2$ efficiency.[22] In order to address this problem, Liu and coworkers[23] reported two AIE conjugated polymers of PTPEDC1 and PTPEDC2 on the basis of the AIE PS unit of TPEDC (Figure 6a). Compared with PTPEDC1, PTPEDC2 has longer polymer conjugation, which would be beneficial to enhance the 2PA cross-section. Indeed, the experimental results showed that 2PA cross-section and $^1O_2$ generation efficiency were in the order of PTPEDC2, PTPEDC1, and TPEDC. Furthermore, the time-dependent density functional theory study revealed that compared with low mass molecules, the special π-conjugated backbone of PTPEDC1 and PTPEDC2 offered them with denser energy levels of both singlet and triplet states, which could increase the ISC channels to facilitate more $^1O_2$ generation. In addition, PTPEDC2 had much denser energy levels and planner conjugation than PTPEDC1, and in turn the 2PA cross-section and $^1O_2$ generation efficiency of PTPEDC2 was better than those of PTPEDC1 (Figure 6b). Subsequently, the authors conjugated a cell penetrating peptide TAT-SH on the surface of PTPEDC2 and realized the efficient ablation of HeLa cells *in vitro* (Figure 6c) and zebrafish liver tumor treatment by 2PE-PDT (Figure 6d). These two AIE conjugated polymers with enhanced two-photon photosensitization provide insight into developing highly efficient photosensitizers for 2PE-PDT.

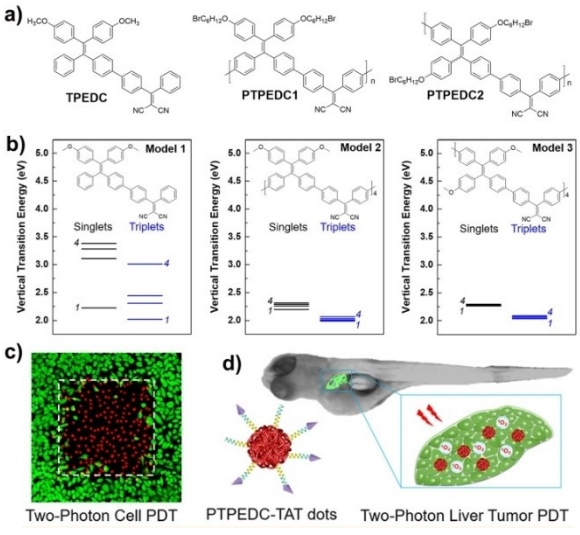

Figure 6. Two-photon excited PDT. (a) Molecular structure of TPEDC, AIE conjugated polymers PTPEDC1 and PTPEDC2. (b) Singlet and triplet energy levels of three model compounds. (c and d) Two-photon cell and liver tumor PDT with PTPEDC2-TAT dots. Reproduced with permission from Ref. [23]. Copyright (American Chemical Society), 2019.

2.4. AIE conjugated polymers in antibacterial applications

In addition to cancer, pathogenic bacteria have also been haunting human lives. It is highly desirable to develop PSs with high-performance to fight against the antibiotic-resistant strains of bacteria.[24] Combination of AIE unit and D-π-A conjugated structure, our group designed and synthesized an AIE conjugated polymer PTB-APFB for reliable bacterial eradication.[25] Introducing the D-π-A structure to the conjugated backbone and incorporating 4-azidoperfluorobenzoate (APFB) moiety in the side chain enabled PTB-APFB to generate ROS effectively. The quaternary ammonium group in the middle instead of the end of the side chains endowed the polymer with appropriate hydrophilicity and selective binding ability toward bacteria over mammalian cells (Figure 7a). The experimental results showed that PTB-APFB had high ROS-generation ability under both white light and sunlight, and the ROS generation ability could be greatly enhanced especially upon formation of aggregates. Compared with a low mass model compound of MTBAPFB and the commercial photosensitizer of Ce6, PTB-APFB had a 13- and 11-fold improvement in ROS generation capability (Figure 7b), respectively. Moreover, the results of CLSM demonstrated that PTB-APFB could bind with *S. aureus* (gram-positive bacteria), *E. coli* (gram-negative bacteria) and *C. albicans* (fungi) effectively, especially toward *S. aureus*, but showed relatively weak binding affinity with HeLa cells (Figure 7c and 7d). This selectivity might be attributed to following reasons: the positively charged side chains of PTB-APFB that make it readily bind with micro-organisms through electrostatic interaction, and the balanced hydrophilicity and hydrophobicity that hinder it to bind with the cells. Furthermore, PTB-APFB could inhibit the growth of *S. aureus* with 100% efficiency under white light irradiation or sunlight (Figure 7e). Subsequently, inflammation model experiments validated that PTB-APFB could effectively inhibit the growth of bacteria to promote the healing rate, which was quicker than that of commercial Cefalotin (Figure 7f-h). Therefore, this work would be a valuable reference for preparing AIE conjugated polymers with both good biocompatibility and high ROS-generation efficiency as antibacterial agent for preclinical research and clinical applications.

3. Conclusions

In this review, we briefly summarize the progress of the application of AIE conjugated polymers in anticancer and antibacterial areas. AIE conjugated polymers possess the advantages of both AIEgens and conjugated polymers. Because of the introduced AIE units and conjugated structures, the fluorescence intensity and QYs of AIE conjugated polymers could be greatly improved, and the fluorescent emission could

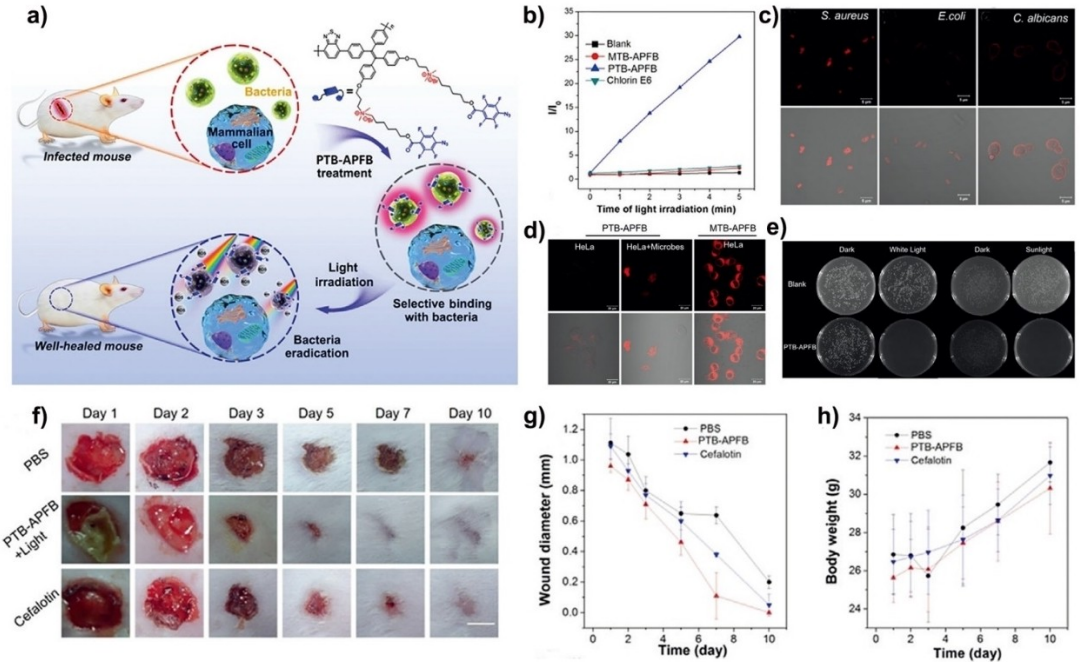

Figure 7. The application of AIE conjugated polymers for antibacterial therapy. (a) Chemical structure of PTB-APFB and its selective antibacterial application. (b) Relative fluorescence intensity of 2′,7′-dichlorofluorescein (DCFH) in PTB-APFB, MTB-APFB, and Ce 6 under white light exposure (10 mW/cm^2), respectively. (c) Confocal laser scanning microscopy (CLSM) of *S. aureus*, *E. coli*, and *C. albicans* samples incubated with PTBAPFB, respectively. (d) CLSM images of HeLa cells and mixed sample (HeLa cells + microorganisms) incubated with PTB-APFB or MTB-APFB, respectively. (e) Photographs of NB agar plate of *S. aureus* with PTB-APFB treatment in dark, and under white light and sunlight. (f) Photographs of the *S. aureus*-infected skin of mice during treatment with the different formulations. (g and h). The size of the infected area and body weight of PBS, PTB-APFB, Cefalotin groups, respectively. Reproduced with permission from Ref. [24]. Copyright (John Wiley & Sons Inc.), 2020.

be tuned from green to NIR. The advantages of AIE conjugated polymers could be briefly concluded as following: 1) Strong D-π-A conjugated structure can not only separate the energy levels of the highest-energy occupied molecular orbital (HOMO) from the lowest-energy unoccupied molecular orbital (LUMO), but also reduce the $\Delta E_{S\text{-}T}$ between the lowest singlet level (S_1) and the lowest triplet level (T_1), which is effective for ROS generation. 2) The extended π-conjugation backbone can not only provide a straightforward platform for efficient energy transfer to realize the color-tuned FLI, but also make the energy levels in different energy bands much denser to approach S_1 and T_1, which can promote more ISC process not just S_1 to T_1, leading to more $^1O_2$ generation. 3) The AIE moiety can guarantee simultaneously the photo-stability and high $^1O_2$ generation ability compared with the traditional conjugated polymers. Therefore, AIE conjugated polymers hold great potential for imaging and photodynamic therapy applications. Moreover, the AIE conjugated polymers could also enhance the tissue penetration depth by two-photon excitation, which can directly improve the efficiency of 2PE-PDT.

As aforementioned, although remarkable progress has been achieved in this area, there are still some problems to be address. First, for *in vivo* applications, the light penetration depth is a vital factor for imaging-guided PDT. Apart from two-photon excitation, chemiluminescence would be alternative strategy to conquer tissue penetration depth.[26] If chemiluminescence-guided PDT could be applied in tumor, that would be a meaningful direction for AIE conjugated polymers. Second, good biodegradability is beneficial to *in vivo* biosafety for conjugated polymers. Therefore, developing novel AIE conjugated polymers with good biocompatibility and biodegradability for *in vivo* application is the future development direction. Third, most of AIE conjugated polymers are hydrophobic, which are generally encapsulated into biocompatible nanoparticles for *in vivo* application. This provides an opportunity for construction of multifunctional AIE conjugated polymers nanoparticles by encapsulating drugs, catalytic enzyme, and other imaging contrast agents to realize the chemotherapy/PDT integrated therapy, overcoming the hypoxic environment, and multimodal imaging-guided PDT *etc.*

Acknowledgements

This work was financially supported by the National Natural Science Foundation of China (21788102 and 51620105009), the Natural Science Foundation of Guangdong Province (2019B030301003, 2019A1515012144 and 2016A030312002), the National Key Research and Development Program of China (Intergovernmental cooperation project, 2017YFE0132200), and the Innovation and Technology Commission of Hong Kong (ITC-CNERC14S01). L. Wang thanks the support by the Fundamental Research Funds for the Central Universities (2019MS008) and the China Postdoctoral Science Foundation Grant (2019M652887). We

are very grateful to Dr. Ni Kaiyuan for proof reading of this manuscript.

Conflict of Interest

The authors declare no conflict of interest.

Keywords: AIE conjugated polymers · color-tuned fluorescent emission · reactive oxygen species · photodynamic therapy · antibacterial agents

[1] a) A. Langdon, N. Crook, G. Dantas, *Genome Med.* **2016**, *8*, 39; b) F. Bray, J. Ferlay, I. Soerjomataram, R. L. Siegel, L. A. Torre, A. Jemal, *Ca-Cancer J. Clin.* **2018**, *68*, 394–424.
[2] a) B. Yang, Y. Chen, J. Shi, *Chem. Rev.* **2019**, *119*, 4881–4985; b) F. Hu, S. Xu, B. Liu, *Adv. Mater.* **2018**, *30*, e1801350; c) Z. Zhou, J. Song, L. Nie, X. Chen, *Chem. Soc. Rev.* **2016**, *45*, 6597–6626; d) J. Hu, W. Jiang, L. Yuan, C. Duan, Q. Yuan, Z. Long, X. Lou, F. Xia, *Aggregate* **2021**, *2*, 48; e) Q. Wan, R. Zhang, Z. Zhuang, Y. Li, Y. Huang, Z. Wang, W. Zhang, J. Hou, B. Z. Tang, *Adv. Funct. Mater.* **2020**, 2002057; f) Z. Zhuang, J. Dai, M. Yu, J. Li, P. Shen, R. Hu, X. Lou, Z. Zhao, B. Z. Tang, *Chem. Sci.* **2020**, *11*, 3405–3417.
[3] R. Baskaran, J. Lee, S. G. Yang, *Biomater. Res.* **2018**, *22*, 25.
[4] a) S. Singh, A. Aggarwal, N. V. Bhupathiraju, G. Arianna, K. Tiwari, C. M. Drain, *Chem. Rev.* **2015**, *115*, 10261–10306; b) K. Liu, Y. Liu, Y. Yao, H. Yuan, S. Wang, Z. Wang, X. Zhang, *Angew. Chem. Int. Ed.* **2013**, *52*, 8285–8289; *Angew. Chem.* **2013**, *125*, 8443–8447.
[5] a) X. Fu, H. Bai, F. Lyu, L. Liu, S. Wang, *Chem. Res. Chin. Univ.* **2020**, *36*, 237–242; b) F. Peng, L. Qiu, R. Chai, F. Meng, C. Yan, Y. Chen, J. Qi, Y. Zhan, C. Xing, *Macromol. Chem. Phys.* **2018**, *219*, 1700440; c) Z. Meng, W. Hou, H. Zhou, L. Zhou, H. Chen, C. Wu, *Macromol. Rapid Commun.* **2018**, *39*, 1700614; d) W. Wu, G. C. Bazan, B. Liu, *Chem.* **2017**, *2*, 760–790; e) C. G. Qian, Y. L. Chen, P. J. Feng, X. Z. Xiao, M. Dong, J. C. Yu, Q. Y. Hu, Q. D. Shen, Z. Gu, *Acta. Pharmacol. Sin.* **2017**, *38*, 764–781.
[6] W. Wu, G. Feng, S. Xu, B. Liu, *Macromolecules* **2016**, *49*, 5017–5025.
[7] a) D. Wang, B. Z. Tang, *Acc. Chem. Res.* **2019**, *52*, 2559–2570; b) X. Cai, B. Liu, *Angew. Chem. Int. Ed.* **2020**, *59*, 9868–9886; *Angew. Chem.* **2020**, *132*, 9952–9970; c) J. Li, J. Wang, H. Li, N. Song, D. Wang, B. Z. Tang, *Chem. Soc. Rev.* **2020**, *49*, 1144–1172.
[8] a) C. Chen, H. Ou, R. Liu, D. Ding, *Adv. Mater.* **2020**, *32*, e1806331; b) M. Kang, Z. Zhang, N. Song, M. Li, P. Sun, X. Chen, D. Wang, B. Z. Tang, *Aggregate* **2020**, *1*, 80.
[9] a) G. Feng, B. Liu, *Acc. Chem. Res.* **2018**, *51*, 1404–1414; b) S. Wang, H. Chen, J. Liu, C. Chen, B. Liu, *Adv. Funct. Mater.* **2020**, 2002546; c) R. Hu, Q. Deng, Q. Tang, R. Zhang, L. Wang, B. Situ, C. Gui, Z. Wang, B. Z. Tang, *Biomaterials* **2021**, *271*, 120725; d) J. Dai, X. Wu, S. Ding, X. Lou, F. Xia, S. Wang, Y. Hong, *J. Med. Chem.* **2020**, *63*, 1996–2012; e) W. Zhang, Y. Huang, Y. Chen, E. Zhao, Y. Hong, S. Chen, J. W. Y. Lam, Y. Chen, J. Hou, B. Z. Tang, *ACS Appl. Mater. Interfaces* **2019**, *11*, 10567–10577.
[10] a) L. Wang, G. Fang, D. Cao, *J. Macromol. Sci. A.* **2014**, *51*, 668–681; b) R. Hu, A. Qin, B. Z. Tang, *Prog. Polym. Sci.* **2020**, *100*, 101176.
[11] R. Hu, T. Zhou, B. Li, R. T. K. Kwok, J. Shen, A. Qin, B. Z. Tang, *Biomaterials* **2020**, *230*, 119658.
[12] Z. Zheng, T. Zhou, R. Hu, M. Huang, X. Ao, J. Chu, T. Jiang, A. Qin, Z. Zhang, *Bioact. Mater.* **2020**, *5*, 1018–1025.
[13] R. Hu, X. Chen, T. Zhou, H. Si, B. He, R. T. K. Kwok, A. Qin, B. Z. Tang, *Sci. China Chem.* **2019**, *62*, 1198–1203.
[14] Z. Wang, C. Wang, Y. Fang, H. Yuan, Y. Quan, Y. Cheng, *Polym. Chem.* **2018**, *9*, 3205–3214.
[15] Z. Wang, C. Wang, Q. Gan, Y. Cao, H. Yuan, D. Hua, *ACS Appl. Mater. Interfaces* **2019**, *11*, 41853–41861.
[16] Z. Zhang, D. Chen, Z. Liu, D. Wang, J. Guo, J. Zheng, W. Qin, C. Wu, *ACS Appl. Polym. Mater.* **2020**, *2*, 74–79.
[17] W. Wu, *Chem* **2018**, *4*, 1762–1764.
[18] a) L. Wang, H. Lin, X. Chi, C. Sun, J. Huang, X. Tang, H. Chen, X. Luo, Z. Yin, J. Gao, *Small* **2018**, *14*, e1801612; b) H. Yan, W. Shang, X. Sun, L. Zhao, J. Wang, Z. Xiong, J. Yuan, R. Zhang, Q. Huang, K. Wang, B. Li, J. Tian, F. Kang, S.-S. Feng, *Adv. Funct. Mater.* **2018**, *28*, 1705710.
[19] W. Wu, D. Mao, S. Xu, Kenry, F. Hu, X. Li, D. Kong, B. Liu, *Chem* **2018**, *4*, 1937–1951.
[20] S. Liu, H. Zhang, Y. Li, J. Liu, L. Du, M. Chen, R. T. K. Kwok, J. W. Y. Lam, D. L. Phillips, B. Z. Tang, *Angew. Chem. Int. Ed.* **2018**, *57*, 15189–15193; *Angew. Chem.* **2018**, *130*, 15409–15413.
[21] J. G. Croissant, J. I. Zink, L. Raehm, J. O. Durand, *Adv. Healthcare Mater.* **2018**, *7*, e1701248.
[22] B. Gu, W. Wu, G. Xu, G. Feng, F. Yin, P. H. J. Chong, J. Qu, K. T. Yong, B. Liu, *Adv. Mater.* **2017**, *29*.
[23] S. Wang, W. Wu, P. Manghnani, S. Xu, Y. Wang, C. C. Goh, L. G. Ng, B. Liu, *ACS Nano* **2019**, *13*, 3095–3105.
[24] C. Yang, C. Ren, J. Zhou, J. Liu, Y. Zhang, F. Huang, D. Ding, B. Xu, J. Liu, *Angew. Chem. Int. Ed.* **2017**, *56*, 2356–2360; *Angew. Chem.* **2017**, *129*, 2396–2400.
[25] T. Zhou, R. Hu, L. Wang, Y. Qiu, G. Zhang, Q. Deng, H. Zhang, P. Yin, B. Situ, C. Zhan, A. Qin, B. Z. Tang, *Angew. Chem. Int. Ed.* **2020**, *59*, 9952–9956; *Angew. Chem.* **2020**, *132*, 10038–10042.
[26] D. Mao, W. Wu, S. Ji, C. Chen, F. Hu, D. Kong, D. Ding, B. Liu, *Chem* **2017**, *3*, 991–1007.

Manuscript received: February 25, 2021
Accepted manuscript online: April 21, 2021
Version of record online: May 10, 2021